Journal of Earthquake Engineering

ISSN: (Print) (Online) Journal homepage: https://www.tandfonline.com/loi/ueqe20

Displacement Spectra Damping Factors for Preliminary Design of Structures with Hysteretic Energy-Dissipation Devices

Miguel A. Orellana, Sonia E. Ruiz & Ali Rodríguez-Castellanos

To cite this article: Miguel A. Orellana, Sonia E. Ruiz & Ali Rodríguez-Castellanos (2022) Displacement Spectra Damping Factors for Preliminary Design of Structures with Hysteretic Energy-Dissipation Devices, Journal of Earthquake Engineering, 26:12, 6260-6283, DOI: 10.1080/13632469.2021.1913455

To link to this article: https://doi.org/10.1080/13632469.2021.1913455

Published online: 22 Apr 2021.

JOURNAL OF EARTHQUAKE ENGINEERING
2022, VOL. 26, NO. 12, 6260–6283
https://doi.org/10.1080/13632469.2021.1913455

Displacement Spectra Damping Factors for Preliminary Design of Structures with Hysteretic Energy-Dissipation Devices

Miguel A. Orellana, Sonia E. Ruiz, and Ali Rodríguez-Castellanos

Structural Engineering Department, Instituto de Ingeniería, Universidad Nacional Autonoma de Mexico, Mexico City, Mexico

ABSTRACT

A methodology based on probabilistic seismic risk analysis to estimate damping factors (F_{md}) which modify the spectrum of elastic displacement with uniform annual exceedance rates (UAER), is proposed. Such factors take into account both a) energy dissipation of the hysteretic dissipaters and b) seismic hazard of the site. It is shown the importance of taking into account the type of soil for a proper selection of the dissipater characteristics. Mathematical expressions for F_{md} factors are proposed. An example in which F_{md} factors are applied using a displacement-based design approach is presented. The results are verified with time-history analyses.

ARTICLE HISTORY
Received 2 March 2020
Accepted 1 April 2021

KEYWORDS
Probabilistic seismic risk analysis; PSRA; hysteretic energy dampers; damping factors; displacement spectra; displacement-based design

1. Introduction

Several recent earthquakes have brought up the limitations of the traditional philosophy of seismic design in which, when facing an intense seismic event, buildings must not collapse, with the objective of protecting the lives of the occupants. However, it is accepted that structures undergo some damage, or get tolerable permanent residual deformations. Even though the structure complies with the objectives of seismic design, the damage is often so significant that it is required to interrupt the activities in the building, or even to demolish it (Fukuyama and Sugano 2000), thus provoking big economic losses. Moreover, damage and important losses in both content and non-structural elements may be generated.

Based on what is stated above, performance-based seismic design criteria that establish several performance levels quantified in terms of damage, according to different levels of seismic demand have been proposed. Currently, the concept of performance-based seismic design is still evolving, as shown by Liu, Liu, and Li (2004), Moehle and Deierlein (2004), Yang et al. (2009), Zeng et al. (2016), FEMA P-58-1 (2018). Some of these documents contain concepts in which seismic performance consists not only in obtaining the performance level associated to an expected damage level, but also in including indicators of seismic performance during the life-cycle of the structures, such as time of interruption of activities, reconstruction, economic loss, risk of injuries, and life loss.

Regarding this topic, the new philosophies of seismic design aim to have more resilient structures (quick recovery capacity). As an alternative, the inclusion of seismic protection systems in structures through the use of energy dissipaters has been promoted over the last few decades. Examples of such devices are the classical steel dampers whose energy dissipation depends on the displacement between its ends (Merritt, Uang, and Benzoni 2003) as well as new replaceable dampers that reduce architectural invasiveness, such as Dissipative Columns (DC) consisting of two or more adjacent steel vertical elements connected with continuous mild/low strength steel X-shaped plates (Palazzo, Castaldo, and Marino 2015). The objective of such damping systems is to absorb most of the seismic energy through

CONTACT Sonia E. Ruiz sruizg@iingen.unam.mx Structural Engineering Department, Instituto de Ingeniería, Universidad Nacional Autonoma de Mexico, Mexico City, Mexico.

its non-linear inelastic structural behavior (hysteretic). In addition, hysteretic dampers such as buckling restrained braces (BRBs) represent one of the best solutions for retrofitting or upgrading the numerous existing buildings in areas with a high seismic hazard (Castaldo et al. 2021; Ruiz et al. 2021). Currently, there are multiple buildings equipped with hysteretic dampers around the world (Domínguez and López-Almansa 2017; Symans et al. 2008; Takeuchi 2018).

Hysteretic dampers are activated through relative displacement between their ends, which makes them particularly appropriate for design using procedures based on displacement control. Furthermore, structural damage caused by seismic events is more directly related to both displacements and deformations of structural elements, rather than to the forces. Priestley, Calvi, and Kowalsky (2007) present a design method based on direct displacement (DBDD) applicable to conventional structures with both regular mass and regular geometry over their height, in which the response is dominated by the fundamental vibration mode. In this methodology, it is common practice to assign the system an equivalent viscous damping (EVD) representative of the inherent damping, the supplementary damping and the hysteretic energy absorbed during the inelastic response; thus, EVD allows the reduction of the displacement spectrum of seismic design. Some studies have extended the displacement-based seismic design methodology to the design of buildings equipped with hysteretic dissipaters (Kim and Seo 2004; Maley, Sullivan, and Della Corte 2010; Segovia and Ruiz 2017).

For the displacement-based design of systems with hysteretic dissipaters, it is necessary to properly modify the elastic displacement design spectrum, due to the energy dissipation of the damper. Inoue and Kuwara (1998) propose an expression to estimate EVD for systems equipped with hysteretic dissipaters. On the other hand, Castillo and Ruiz (2014) recommend to directly modify the acceleration design spectrum with a factor that takes into account the supplementary damping given by the hysteretic dissipater.

Most seismic design guidelines around the world (BCJ 1997; CEN 2004; NRCC 2010; ASCE 2016; MCBC 2017) consider design methodologies compatible with the use of either response spectra or design spectra, and allow the modification of design acceleration spectral ordinates through different factors, i.e., ductility factors, over-strength factors, damping factors, etc. There are several studies that propose damping factors to modify seismic spectral ordinates due to supplementary damping given to the structure (Kawashima and Aizawa 1986; Ashour 1987; Tolis and Faccioli 1999; Bommer, Elnashai, and Weir 2000; Naeim and Kircher 2001; Arroyo-Espinoza and Terán-Gilmore 2002; Zhou, Wenguang, and Xu 2003; Bommer and Mendis 2004; Cameron and Green 2007; Hidalgo and Ruiz 2010; Hatzigeorgiou 2010; Papagiannopoulos, Hatzigeorgiou, and Beskos 2013; Castillo and Ruiz 2014; Mollaioli, Liberatore, and Lucchini 2014; Nagao and Kanda 2015; Hazaveh et al. 2016; Palermo, Silvestri, and Trombetti 2016; Greco, Fiore, and Briseghella 2018; Zhou and Zhao 2020; etc.); however, such damping factors are applicable to systems with viscous dissipaters.

In the literature, there are also studies that suggest over-strength and ductility modification factors for systems equipped with hysteretic dissipaters (Abdollahzadeh, Elkaee, and Esmaeelnia 2012; Asgarian and Shokrgozar 2009). However, such studies are applied to a limited number of systems and do not propose modification factors for the displacement spectrum.

Considering what is stated above, it is inferred that it is important to count on factors that both 1) allow modifying the seismic design displacement spectra due to the presence of hysteretic dissipaters in the structural system, and 2) are compatible with displacement-based seismic design approaches. Therefore, in the present study, a methodology to obtain mathematical expressions to estimate damping factors to directly modify the seismic design displacement spectra is proposed; both the hysteretic energy dissipation and the dynamic characteristics of the soil on which structures are located are considered. It is shown that the efficiency of the dissipaters varies according to the characteristics of the ground motion (effective duration and frequency content). Also, it is proved that the proper selection of the dissipater characteristics depends on the type of soil where the structure is located. Furthermore, an illustrative example in which damping factors are applied using a displacement-based design approach is presented.

2. Equations that govern a single-degree-of-freedom (SDOF) system equipped with hysteretic dissipaters

1.1. Simple SDOF System

The seismic response of a single-degree-of-freedom (SDOF) system considering non-linear behavior can be calculated using the following equation (Sues, Mau, and Wen 1988):

$$\mathrm{m}\,\ddot{u} + c\dot{u} + \delta k u + (1-\delta)kz = -m\ddot{u}_g \tag{1}$$

where m is the mass, *c* is the viscous damping coefficient, and *k* is the lateral stiffness of the system; $\ddot{u}$, $\dot{\mathrm{u}}$ and u are acceleration, velocity and displacement of the mass with respect to the base, respectively; $\ddot{u}_g$ *is the acceleration at the base of the system, and z* is the hysteretic component with units of displacement; δku and *(1-δ)kz* represent the restoring force that depends on both the displacement u and the hysteretic component *z*, respectively. The hysteretic component is obtained by modeling the hysteretic cycles through a first-order differential equation. Such equation, capable of considering material degradation, is given by (Baber and Wen 1981):

$$\dot{\mathrm{z}} = \frac{A\dot{\mathrm{u}} - \nu\left(\beta|\dot{\mathrm{u}}||\mathrm{z}|^{\mathrm{n}-1}\mathrm{z} + \lambda\dot{\mathrm{u}}|\mathrm{z}|^{\mathrm{n}}\right)}{\eta} \tag{2}$$

where *A*, *β*, *λ* and *n* are parameters that control amplitude, shape of the hysteretic cycle, and the transition smoothness from the elastic to the inelastic range; *η* and *ν* are parameters that control stiffness and strength degradation, respectively. Parameter *δ* in Eq. (1) represents the ratio between post-yielding stiffness and the initial stiffness of the system (*k*), when *A* = 1.

For non-linear models without considering stiffness and strength degradation of steel elements, it can be considered that *β* = *λ* (Sues, Mau, and Wen 1988). For steel elements, parameter *λ* is obtained through the following equation (Casciati and Faravelli 1991; Silva and Ruiz 2000):

$$\lambda = \frac{1}{2\nu}\left(\frac{\mathrm{k}}{\mathrm{V_y}}\right)^{\mathrm{n}} \tag{3}$$

where V_y is the force at which a perfect elasto-plastic system yields.

1.2. Dual SDOF System

The dual system, or structure-dissipater system (Fig. 1a) is considered to be constituted by two subsystems: 1) a primary structural system (which are commonly flexural moment resisting frames capable of holding at least gravitational forces), and 2) a secondary system, which is composed by

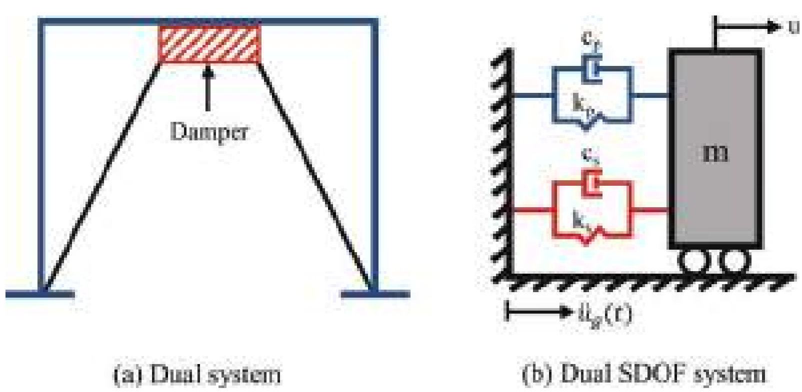

Figure 1. Model of a dual system.

energy dissipation elements. The latter is normally designed to resist lateral forces and must dissipate important amounts of energy through yielding on both directions (in the case of hysteretic dissipaters). A desirable seismic behavior of the dual structure is that the primary system does not enter into the inelastic range, and that all energy dissipation concentrates on the secondary system. This behavior can be achieved by limitating the deformation level of the dual structure; that is, by controlling the displacement demand in order to avoid damage to the primary system (Segovia and Ruiz 2017; Teran-Gilmore and Virto-Cambray 2009; Vargas and Bruneau 2009).

The model corresponding to the dual system can be characterized in a simplified way as a SDOF plus a parallel secondary element that represents the seismic energy dissipater (Guerrero et al. 2016; Nakashima, Saburi, and Tsuji 1996; Ruiz and Badillo 2001), as shown in Fig. 1b. Figure 2 shows capacity curves of the primary, secondary and dual systems in a schematic way. In Fig. 2, the term k represents lateral stiffness, and V is the system strength. Subscripts p, s and t refer to the primary, secondary, and dual (total) system, respectively; subscript y indicates the yielding of the systems, and d_{max} the maximum displacement.

The stiffness and strength ratios of the dual system are defined through parameters α and γ, respectively. The first (α) is the ratio between the stiffness of the primary system k_p and that of the dual system k_t (Eq. 4), and γ is the ratio between the yielding force of dissipater (secondary system) V_{ys} and the yielding force of the dual system V_{yt} (Eq. 5).

$$\alpha = \frac{k_p}{k_t} \tag{4}$$

$$\gamma = \frac{V_{ys}}{V_{yt}} \tag{5}$$

The properties of stiffness and strength of the dual (total) system are obtained by adding the properties of the primary and the energy dissipation system (secondary system). Thus, the values of the total stiffness and the total strength of the system are given by Eqs. (6) and (7), respectively:

$$k_t = k_p + k_s \tag{6}$$

$$V_{yt} = V_{yp} + V_{ys} \tag{7}$$

Substituting Eq. (7) in Eq. (5) yields V_{ys} as a function of γ and V_{yp}, as follows:

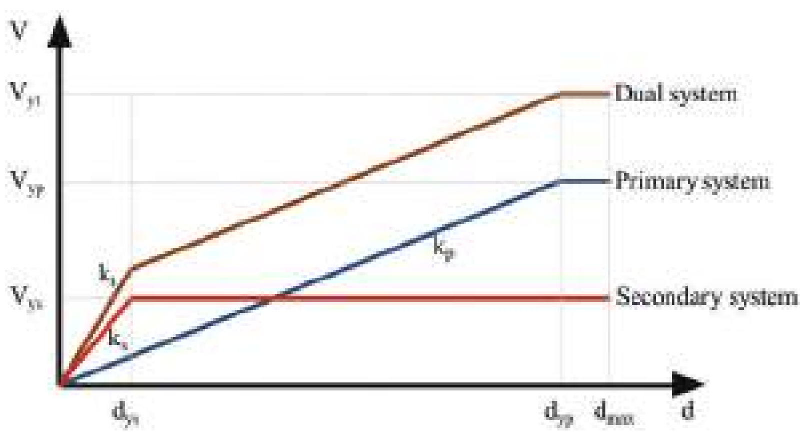

Figure 2. Capacity curves.

$$V_{ys} = \frac{V_{yp}\gamma}{1-\gamma} \tag{8}$$

On the other hand, through Eq. (1) and Fig. 1b, the response of a dual SDOF system to a seismic excitation, considering non-linear behavior in both the conventional system and the energy dissipater, :

$$\mathrm{m}\,\ddot{u} + \mathrm{c_t}\,\ddot{u} + \delta_\mathrm{p}\mathrm{k_p u} + \left(1-\delta_\mathrm{p}\right)\mathrm{k_p z_p} + \delta_\mathrm{s}\mathrm{k_s u} + (1-\delta_\mathrm{s})\mathrm{k_s z_s} = -\mathrm{m}\ddot{u}_\mathrm{g} \tag{9}$$

In this case, the total restoring force is given by the contribution of both the restoring force of the primary system (terms with subscript p) and the dissipater (terms with subscript s).

The hysteretic components are obtained representing the hysteretic cycles with a first-order differential equation. The differential equations of both the conventional system and the dissipater are, respectively (Baber and Wen 1981; Rivera and Ruiz 2007):

$$\dot{z}_p = \frac{A_p\dot{u} - \nu_p\left(\beta_p|\dot{u}||z_p|^{n_p-1}z_p + \lambda_p\dot{u}|z_p|^{n_p}\right)}{\eta_p} \tag{10}$$

$$\dot{z}_s = \frac{A_s\dot{u} - \nu_s\left(\beta_s|\dot{u}||z_s|^{n_s-1}z_s + \lambda_s\dot{u}|z_s|^{n_s}\right)}{\eta_s} \tag{11}$$

Terms A, β, λ, n, η and ν have the same meaning as in Eq. (2).

1.3. Design Parameters

For the analyses of the dual SDOF system, it is assumed that the primary system has linear behavior. Therefore, parameters used are $A_p = n_p = \eta_p = \nu_p = \delta_p = 1$. For the secondary system, a non-linear hysteretic behavior is considered (it is assumed that neither stiffness nor strength degrades) with parameters $A_s = \eta_s = \nu_s = 1$. A smooth transition from the elastic to the inelastic range given by $n_s = 1$ and a post-yielding stiffness– elastic stiffness ratio $\delta_s = 0.025$, are considered. Parameters n_s and δ_s were chosen based on experimental studies by Cameron, Makris, and Aiken (2004) and, Hurtado and Bozzo (2008) for hysteretic dissipaters. $\beta_s = \lambda_s$ according to recommendations by Sues, Mau, and Wen (1988).

Using Eqs. (4)–(7), and considering linear behavior of the primary system ($d_{max} = d_{yp}$), the ductility developed by the dissipater system as a function of parameters α and γ can be expressed as follows:

$$\mu_s = \frac{(1-\alpha)(1-\gamma)}{\alpha\gamma} \tag{12}$$

Eq. (12) shows that the greater the values of α and γ, the lower the ductility demands for the dissipater.

In this study, stiffness ratios of $0.25 \le \alpha \le 0.60$ are assumed (Table 1). The lower limit of the interval is selected in order to avoid having excessively large dimensions in the dissipaters; in addition, this

Table 1. Values of α and γ used in this study.

α	γ
0.25	0.25–0.65
0.30	0.20–0.60
0.35	0.20–0.55
0.40	0.20–0.50
0.45	0.20–0.45
0.50	0.20–0.40
0.55	0.20–0.35
0.60	0.20–0.30

lower limit is recommended for best seismic performance (Vargas and Bruneau 2009); the upper limit is chosen so as to have a significant stiffness contribution of the dissipater system to the total system (Segovia and Ruiz 2017) and also to avoid large beams and columns in the system (Vargas and Bruneau 2006).

The lower limit of the strength ratio γ are chosen based on recommendations given by Segovia and Ruiz (2017) to have a significant strength contribution of the dissipater system to the total system, and the upper limit is determined by means of Eq. 12, where the dissipater is considered to develop ductilities $\mu_s \geq 1.5$, in order to assure that the secondary system dissipates energy. Table 1 shows values of α and γ used in the present study. Notice that in Table 1 the interval of γ values is different for each value of α.

2. General Methodology

In this section, a methodology based on a probabilistic seismic risk analysis (PSRA) is proposed, with the objective of estimating modification factors for the displacement spectra. To do so, the following steps are taken:

(1) The seismic response of multiple SDOF systems corresponding to dual systems equipped with hysteretic dissipaters (dual SDOF system) is obtained. Simultaneously, the response of conventional systems without dissipaters (simple SDOF system) is calculated. Different combinations of the dual systems characteristics and different vibration periods are considered. The characteristics of the dual system are a function of both the stiffness ratios α and the strength ratios γ. Time-history analyses are done in order to calculate the Structural Demand Parameter (SDP) as a function of the Seismic Intensity Measure (SIM) for both the dual SDOF system and the simple SDOF system. For the case of dual SDOF system, it is considered that non-linearity is present only in the secondary system (dissipater).

(2) Both the median (μ_{lnSDP}) and the standard deviation (σ_{lnSDP}) of the natural logarithm of SDP are obtained for every *SIM*.

(3) Fragility curves corresponding to certain specific values of *SDP* are calculated, using the following equation:

$$\mathrm{P}(\mathrm{SDP} > \delta | \mathrm{SIM} = \mathrm{sim}) = 1 - \Phi\left(\frac{\ln\left(\frac{\delta}{\mu_{\ln \mathrm{SDP}}}\right)}{\sigma_{\ln \mathrm{SDP}}}\right) \tag{13}$$

where $\mathrm{P}(SDP > \delta | SIM = sim)$ *is the conditional probability that the value of SDP* exceeds value δ, given an intensity *SIM = sim*. Φ represents the standard normal probability distribution.

(4) The mean annual exceedance rates for certain specific values of *SDP* are obtained for both, the systems equipped with energy dissipaters, and the conventional systems. The following equation (Cornell 1968; Esteva 1967) is used:

$$v_{SDP}(\delta) = \int \left| \frac{dv_{SIM}(sim)}{d(sim)} \right| P(SDP > \delta | SIM = sim) dsim \tag{14}$$

where $v_{SIM}(sim)$ *is the mean annual number that an intensity greater than or equal to sim* occurs, and it is usually represented with seismic hazard curves associated to the vibration period of the structural system (T_1), for a site of interest, as explained later on; however, other intensity measures can be used (Baker and Cornell 2005; Bojorquez et al. 2017). In this study, pseudo-acceleration ($Sa(T_1)$) is considered as *SIM*, and the value of spectral displacement (*D*) is established as *SDP* associated with the fundamental vibration period of the structural system (T_1).

(5) Displacements spectra with Uniform Annual Exceedance Rates (UAER) are built using the structural demand exceedance curves, for a variety of both conventional systems and dual systems with different characteristics.
(6) With the aim of obtaining modification factors of the displacement spectral ordinates, relations between UAER displacement spectra corresponding to dual systems and UAER displacement spectra of conventional systems, are obtained. The spectra correspond to a given return period and a given ratio of critical damping.
(7) As a last step, mathematical expressions corresponding to spectral coefficients are fitted. The expressions proposed are function of the vibration period of the system, the vibration period of the soil, stiffness ratio α and strength ratio γ of the dual system.

The methodology previously described can be applied to any location around the world. In this study, such methodology is applied to Mexico City (CDMX, for its acronym in Spanish), in which there are different types of soil (they range from very soft to firm ground).

On the other hand, Castaldo, Palazzo, and Ferrentino (2016) and, Castaldo et al. (2020) also proposed methodologies to establish relationships between seismic response corresponding to elastic and inelastic systems, based on a probabilistic seismic risk analysis (PSRA) where seismic fragility curves are developed and are integrated with the seismic hazard curves, in order to define structural demand exceedance rate curves.

3. Seismic Ground Motions

In the present study, 360 seismic ground motions recorded at different accelerometric stations located in different types of soil of CDMX were used. Stations correspond to both the accelerographic network of the Center for Instrumentation and Seismic Record, which is a civil association (CIRES for its acronym in Spanish), and the accelerographic network of the Institute of Engineering of the National Autonomous University of Mexico (RAII-UNAM, for its acronym in Spanish). The seismic ground motions correspond to 18 subduction seismic events, with magnitudes greater than or equal to 5.9, focal depths no larger than 40 km, and epicentral distances no larger than 700 km. Table 2 shows the main characteristics of the seismic events (Global CMT); Fig. 3 shows the location of their epicenters.

Both a normal-type baseline correction (Ordaz and Montoya 2014) and a Butterworth type, order 4 bandpass filter were applied to every seismic motion. The bandpass filters had a cut-off frequency from

Table 2. Characteristics of seismic events used.

			Epicenter coordinates		
Event No.	Date	Magnitude	Lat. N	Long. W	Focal depth (km)
1	19/09/1985	8.0	17.91	101.99	21.3
2	21/09/1985	7.5	17.57	101.42	20.8
3	30/04/1986	6.9	18.25	102.92	20.7
4	25/04/1989	6.9	16.83	99.12	15.0
5	31/05/1990	5.9	16.77	100.12	26.0
6	15/05/1993	6.0	16.45	97.92	38.5
7	24/10/1993	6.6	16.77	98.61	21.8
8	14/09/1995	7.3	16.73	98.54	21.8
9	09/10/1995	8.0	19.34	104.80	15.0
10	15/07/1996	6.6	17.50	101.12	22.4
11	03/02/1998	6.3	15.92	96.22	24.0
12	09/08/2000	6.5	18.13	102.39	33.0
13	22/01/2003	7.5	18.86	103.90	26.0
14	20/03/2012	7.5	16.60	98.39	15.4
15	11/04/2012	6.7	18.10	102.97	20.5
16	18/04/2014	7.3	17.55	101.25	18.9
17	08/05/2014	6.5	17.36	100.74	21.3
18	10/05/2014	6.1	17.31	100.82	20.7

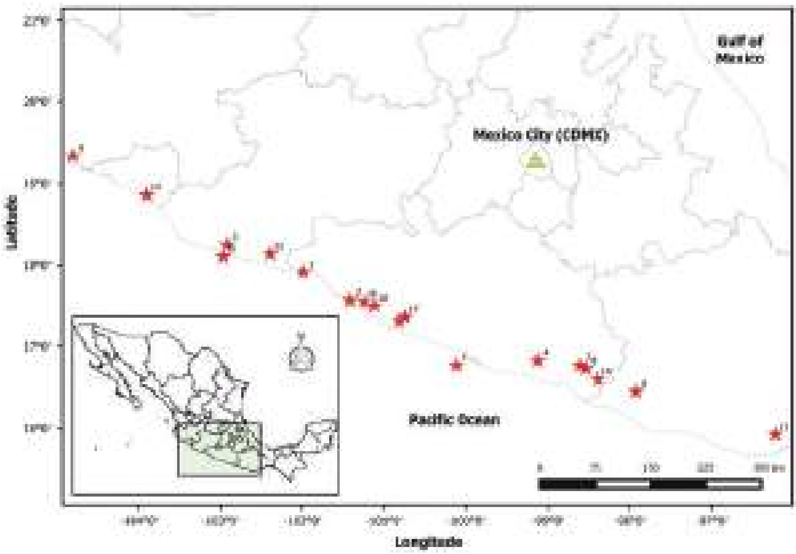

Figure 3. Epicenters of seismic events used in this study.

0.1 to 25 Hz for accelerograms with time-step $\Delta t \leq 0.02$ s. Cut-off frequencies were selected through Fourier spectra. A duration of the seismic motion corresponding to 2.5% and 97.5% of Arias intensity was considered.

Both the pseudo-acceleration elastic spectrum considering 5% of critical damping and its dominant period were calculated for every seismic record. In this study, the Fourier amplitude spectra were used to define the dominant period, which is similar to the period in which the peak ordinate of the pseudo-acceleration spectrum is presented. Such spectrum depends on the type of soil in which the motion is recorded. The ground motions were grouped by zones, according to both the dominant period and the location of the seismic station where the record was obtained. Table 3 shows the seven zones of CDMX considered, with their corresponding intervals of dominant periods of the soil.

Figure 4a–g show the displacement elastic spectra corresponding to each seismic zone. Such figures show the large differences in displacement demands among the zones. The lowest elastic displacement demands are located in zones A, B, and C, corresponding to: A) firm ground formed by rock, B) medium soil formed by silt-sandy strata, intertwined with layers of lacustrine clay, and C) soil with shallow clay strata. On the other hand, the greatest displacement demands are in zones D, E, F, and G, corresponding to soft and very soft soils, formed by highly compressible clay deposits, which can be more than 50 m thick. Shear-wave velocities in the upper 30 m of the hill zone (zone A), transition zone (zone B) and lake-bed zone (zone C to G) are 750, 250, and 50–100 m/s, respectively (Singh et al. 2018). Comparing maximum spectral displacements of zone E and zone A, it can be seen that the differences in the displacement demands for the soft soil zones can be eight times greater than the displacement demands for the firm ground.

Table 3. Seismic zones in CDMX.

Zone	Soil dominant period (T_s)
A	$0< T_s \leq 0.5$
B	$0.5< T_s \leq 1.0$
C	$1.0< T_s \leq 1.5$
D	$1.5< T_s \leq 2.0$
E	$2.0< T_s \leq 2.5$
F	$2.5< T_s \leq 3.0$
G	$3.0< T_s \leq 4.0$

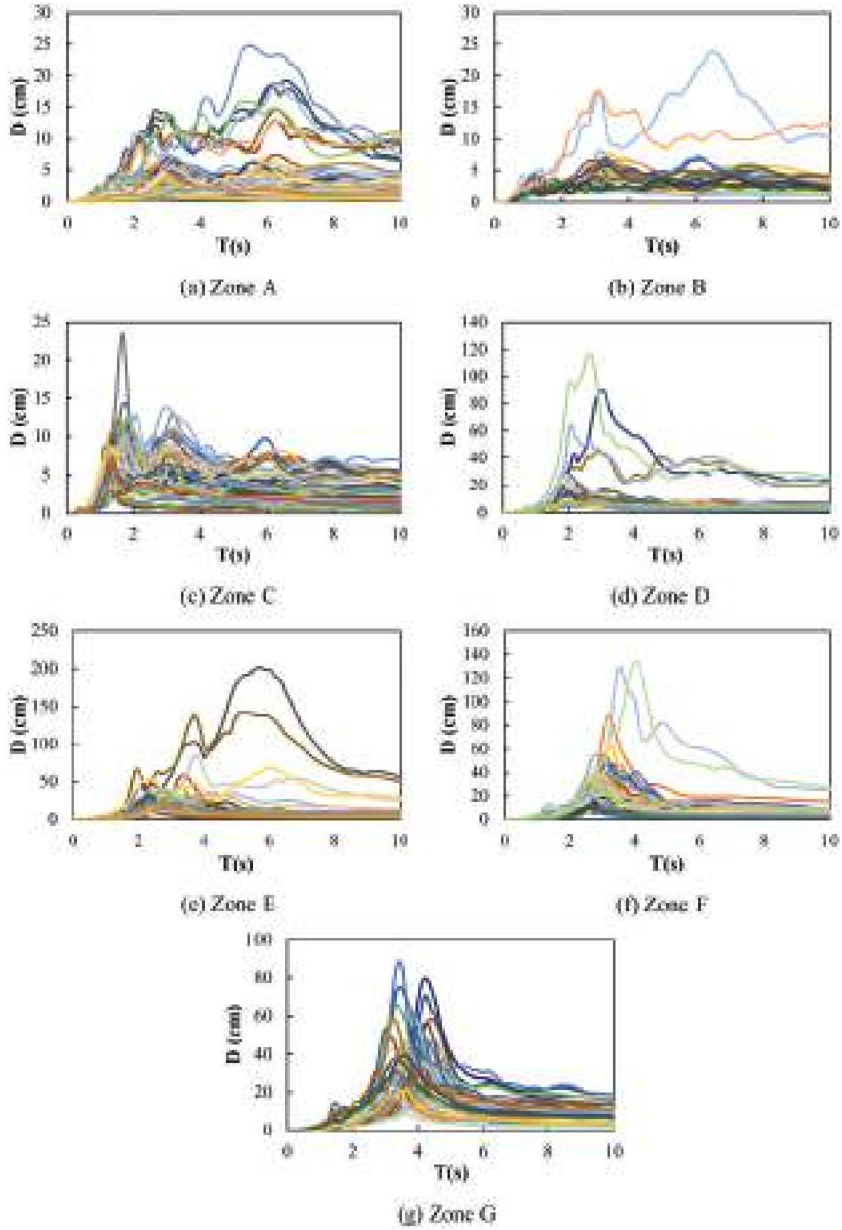

Figure 4. Elastic displacement spectra (ξ = 5%).

Figure 5a–g show the displacement spectra, normalized with respect to their maximum ordinate of each of the seven zones, their averages (with continuous red line), and the normalized average design spectrum obtained in accordance with Mexico City Building Code (MCBC 2017).

Figure 5a–g show that the displacement spectra for zones C, D, E, F and G have a prominent peak; that is, the displacement demands increase until reaching the greatest spectral ordinate, and then tend to decrease until the maximum displacement of the soil is reached. For such zones, the period in which the peak displacement demand occurs is found within the interval of dominant periods of the site (see Table 3). Spectra of zones A and B have different behavior because they have one or more peaks, and

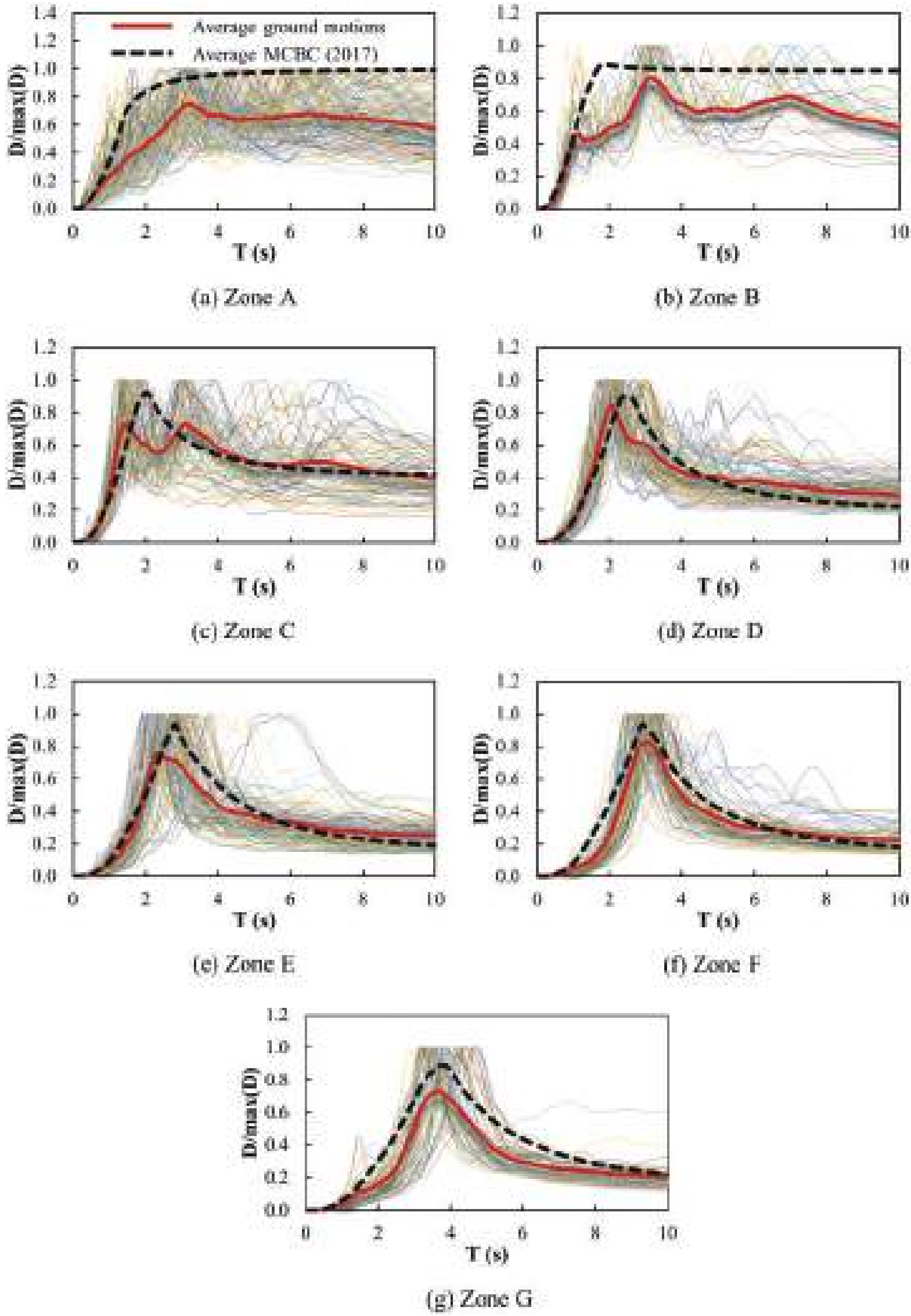

Figure 5. Elastic spectra normalized with respect to their maximum ordinate (ξ = 5%).

the period in which the greatest displacement demand takes place is not found within the interval of dominant periods of the site. So, it is concluded that the type of soil has a significant influence on the demands of elastic displacement of the structures, as expected.

4. Seismic Hazard Curves

Seismic hazard curves represent the mean annual exceedance rates of a certain measure of seismic intensity. In this study, CDMX seismic hazard curves obtained by Castillo and Ruiz (2013) were used. Such curves consider the spectral pseudo-acceleration value (Sa) associated to the vibration period of the structural system (T_1) as seismic intensity. As an example, Fig. 6 shows two seismic hazard curves corresponding to firm ground (zone A) and soft soil (zone D), both corresponding to a structural period T_1 = 2 s. Figure 6 shows the significant influence that the type of soil has on the mean annual exceedance rates of the seismic intensity.

5. Influence of the Design Parameters and the Type of Soil in the Results

Results corresponding to structural systems located in both firm ground (zone A) and soft soil (zone D) are compared in this section in order to illustrate the influence of both the design parameters and the type of soil in: 1) fragility curves, 2) mean annual displacement exceedance curves, 3) UAER displacement spectra, and 4) ratios of UAER displacement spectra.

5.1. Influence of the Type of Soil in Fragility Curves

The calculation of mean annual structural demand exceedance curves requires the calculation of fragility curves (Eq. 13). In this study, a lognormal probability distribution is assumed for the structural response (Rosenblueth and Esteva 1972; Shome and Cornell 1999).

Figure 7a, b show fragility curves for displacement demands (D) of 50 cm and 100 cm for dual systems with T_1 = 2 s, α = 0.30 and γ = 0.40, located in firm ground (zone A) and soft soil (zone D), respectively. Such figures show that the probability of exceeding a given value of displacement demand for a certain intensity is much greater in the systems located in firm ground than in the systems located in soft soil.

Figure 8a, b show fragility curves for a displacement demand of 50 cm for dual systems with T_1 = 2 s, α = 0.30, and different values of γ corresponding to zones A and D, respectively. Such figures show that, for the systems located in firm ground (zone A), and for different levels of seismic intensity, in general, the probability of exceeding a certain value of displacement demand decreases as the value of γ increases; however, the opposite happens for soft soil (zone D).

From this subsection, it is highlighted the influence of the dynamic characteristics of the soil in which the structure is located in the selection of the dissipater characteristics (given by α and γ).

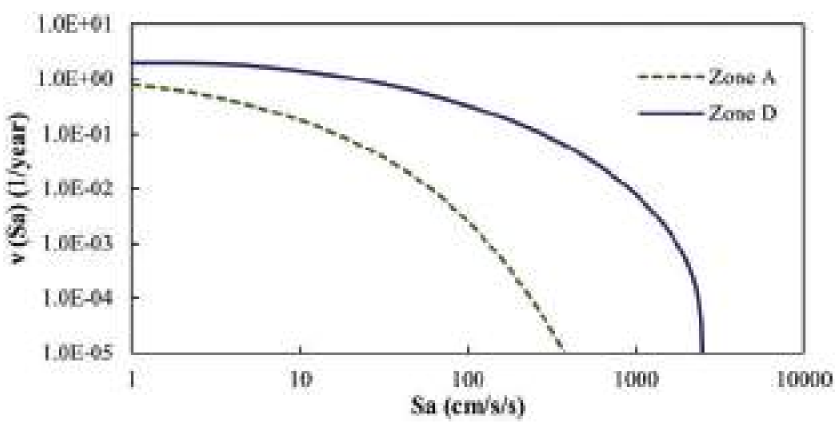

Figure 6. Seismic hazard curves corresponding to T_1 = 2 s.

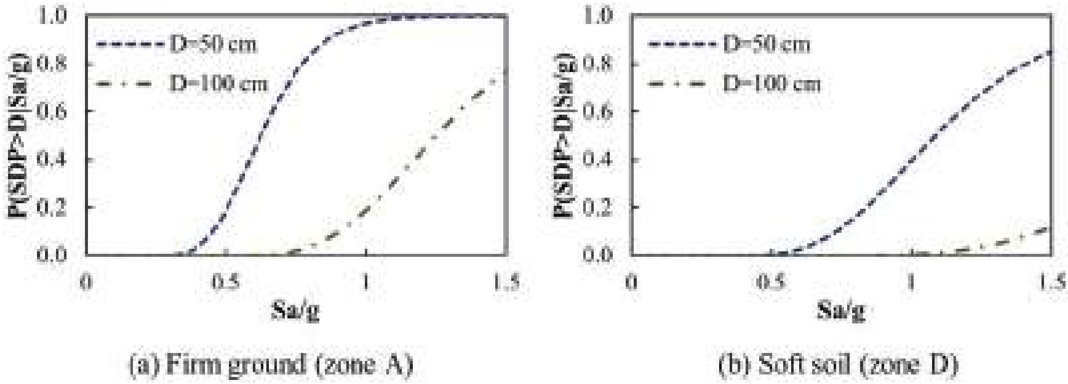

Figure 7. Fragility curves for a dual SDOF system with T_1 = 2 s, α = 0.30 and γ = 0.40.

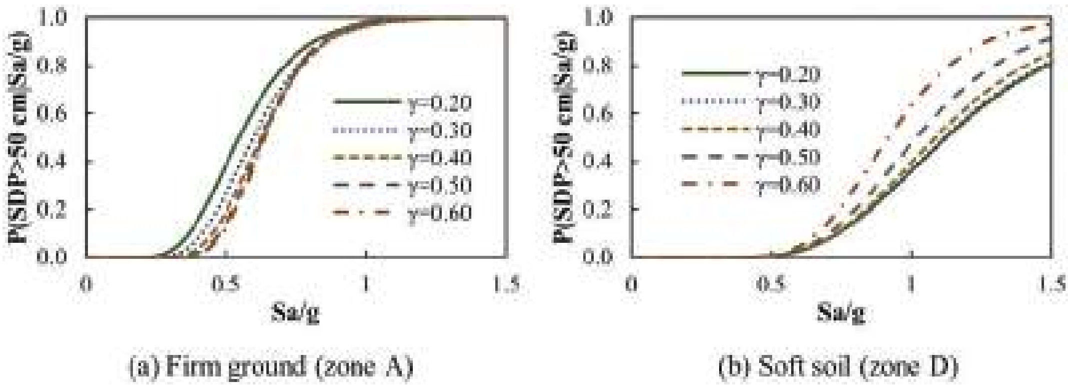

Figure 8. Fragility curves for a dual SDOF system with T_1 = 2 s, α = 0.30 and different values of γ.

5.2. Influence of the Type of Soil in the Mean Annual Displacement Exceedance Curves

Once both the fragility curves and the seismic hazard curves are known, Eq. (14) is applied to estimate the mean annual expected maximum displacement exceedance curves corresponding to systems with different structural vibration periods and different combinations of ratios α and γ. Figure 9a, b show

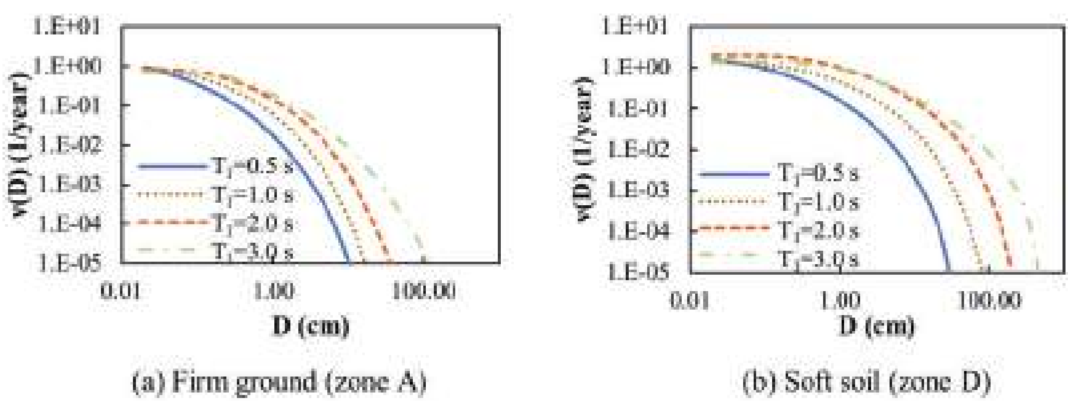

Figure 9. Mean annual displacement exceedance curves for a dual SDOF system with α = 0.30 and γ = 0.40.

mean annual maximum displacement exceedance curves associated to different values of vibration periods for dual systems with α = 0.30 and γ = 0.40 located in firm ground (zone A) and soft soil (zone D), respectively. Such figures show that the displacement exceedance rates for zone D, corresponding to soft soil, are greater than those associated to zone A, corresponding to firm ground.

From this subsection, it is concluded that a greater displacement demand corresponds to the systems located in soft soils, for the same mean annual exceedance rate.

5.3. Influence of Parameters α and γ in the UAER Displacement Spectra

The UAER displacement spectra (which are obtained through mean annual structural demand exceedance curves) contain the maximum ordinates that can be present in a particular site for a given return period T_r (the reciprocal of the exceedance rate ν is T_r).

In this study, the UAER displacement spectra associated to an exceedance rate ν = 0.004, which is equivalent to a return period of 250 years, are obtained. Figures 10 and 11 show, as an example, the UAER displacement spectra for conventional systems (dotted line), and for dual systems (continuous lines), for a structural system considering α = 0.30 and different values of γ, for zones A and D, respectively. Figures 10 and 11 show the following: a) the displacement demands for systems located in firm ground (zone A) are approximately ten times smaller than the demands for the systems located in soft soil (zone D), highlighting the important amplification of the structural response that is present in

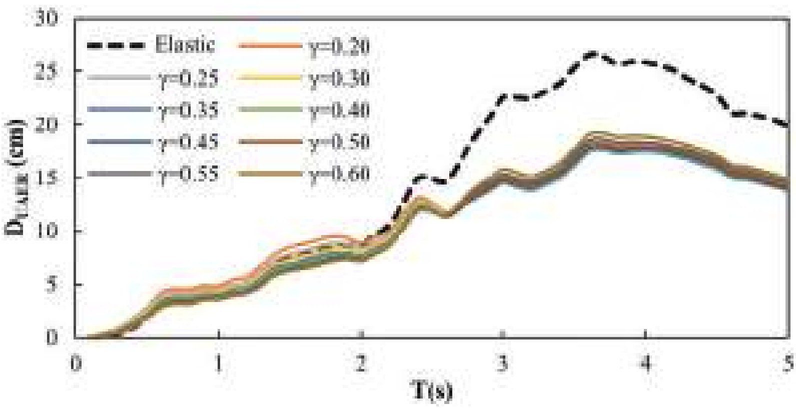

Figure 10. UAER displacement spectra for α = 0.30 and different values of γ, corresponding to firm ground (zone A).

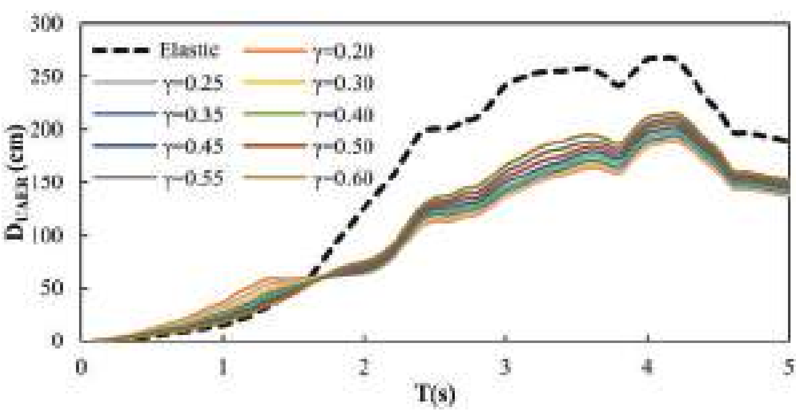

Figure 11. UAER displacement spectra for α = 0.30 and different values of γ, corresponding to soft soil (zone D).

the latter systems, and b) the UAER displacement spectra corresponding to zone A, present smaller differences when changing γ, compared to the differences corresponding to UAER displacement spectra in zone D.

On the other hand, it is observed that, for both zones A and D, the displacement values for dual systems decrease as the value of γ increases, for vibration periods smaller than 2.6 and 1.8 s, respectively. However, for greater periods, such behavior is inverted. Such limit period, herein called *characteristic period* (T_c), is different for each zone.

Figures 12 and 13 show UAER displacement spectra for conventional systems (dotted line) and for dual systems (continuous lines), considering γ = 0.30 and different values of α for zones A and D, respectively. Such figures show that the spectral displacement values for dual systems decrease as the value of α increases, for vibration periods lower than T_c = 2.6s and T_c = 1.8s, respectively. However, for greater periods, such behavior is inverted, as explained later on.

The importance of taking into account the characteristics of the type of soil for a proper selection of the dissipater characteristics (given by α and γ) can be inferred from what is stated above. Such selection of dissipater characteristics has the aim of controlling conveniently the displacement levels required by the structural system; because, when increasing α and γ for a structure on a certain type of soil, the displacements of the structural system can be decreased, whereas the same increase in α and γ for a structure on a different type of soil may result in an increase of the displacement of the structural system. This observation may be important in the design process. Additionally, it is worth mentioning

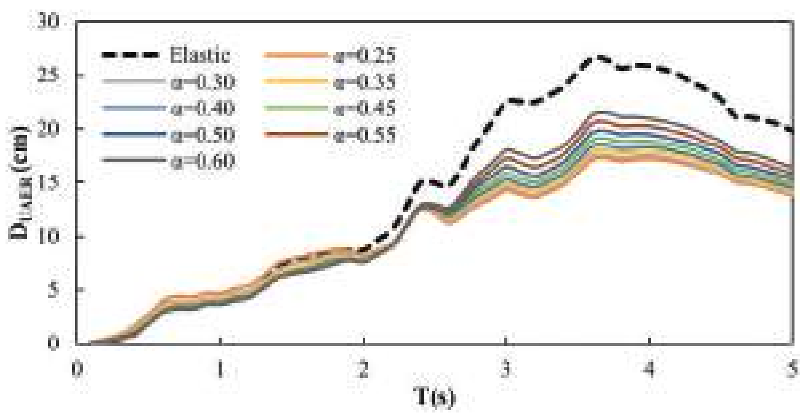

Figure 12. UAER displacement spectra for γ = 0.30 and different values of α, corresponding to firm ground (zone A).

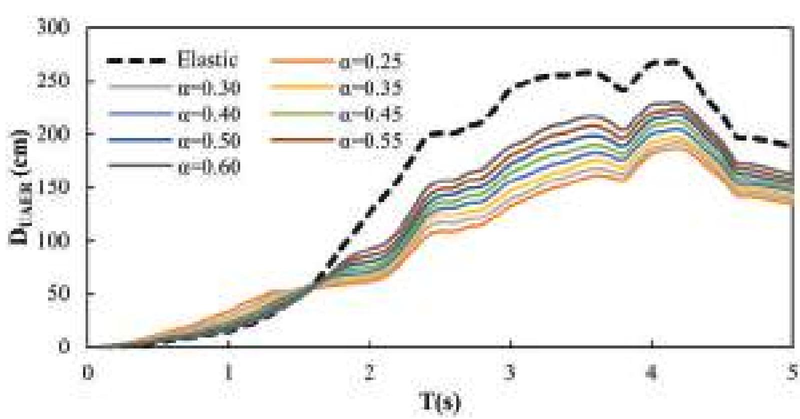

Figure 13. UAER displacement spectra for γ = 0.30 and different values of α, corresponding to soft soil (zone D).

that soil-structure interaction effects were not considered. Consequently, the results might be different from these reported here.

Figure 10–13 show the following: a) the greatest difference among spectral displacement values happens when changing the value of α; b) in general, when increasing the values of α and γ, the inelastic spectrum corresponding to the dual system tends to approximate the elastic spectrum (because both the dissipater capacity and its ductility demands decrease, provoking an inverted behaviour of the displacement after the *characteristic period* T_c when increasing either α or γ); c) the UAER displacement spectra for the dual systems show a behavior similar to the displacement inelastic spectra of conventional systems that develop a constant ductility demand, that is, the inelastic displacement is greater than the elastic displacement in the zone sensitive to acceleration (short periods of vibration); such difference tends to be more significant in systems with greater ductility demands (smaller values of γ). On the other hand, in the zone sensitive to velocity, the inelastic displacement of conventional systems can be either greater or lower than the elastic displacement, because the ductility demand of the system affects the structural behavior irregularly. As for the zone sensitive to displacement (long vibration periods), inelastic displacements tend to be similar to elastic displacements, because the ductility demand of the system is no longer significant.

Figures 14 and 15 show the UAER pseudo-acceleration spectra for conventional systems (dotted line) and dual systems (continuous lines), considering γ = 0.30 and different values of α, for zones A and D, respectively. Such figures also show that, for both firm ground (zone A) and soft soil (zone

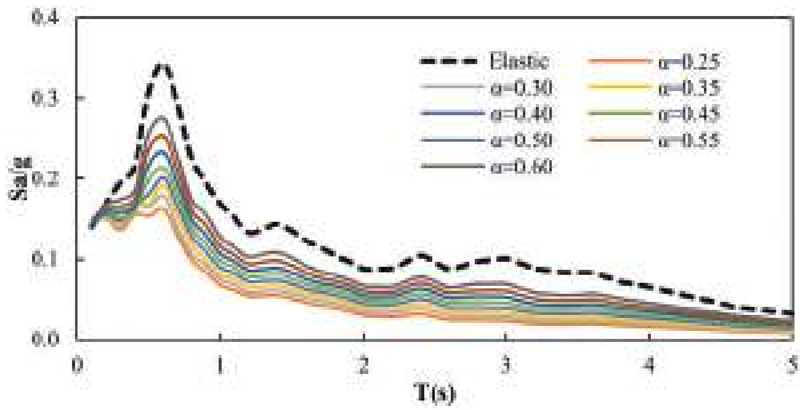

Figure 14. Pseudo-acceleration spectra for γ = 0.30 and different values of α, corresponding to firm ground (zone A).

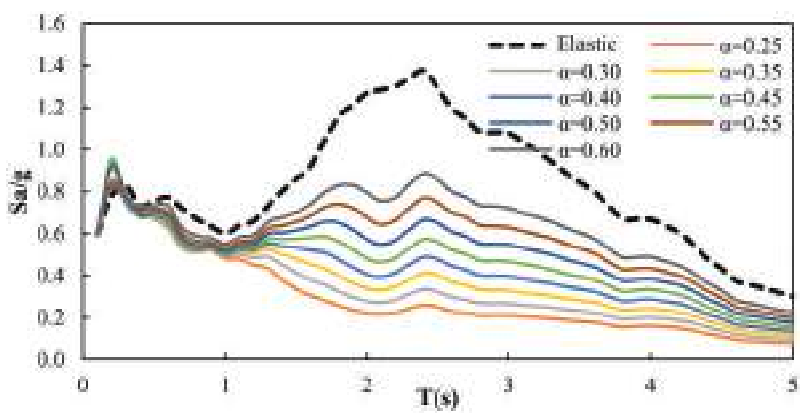

Figure 15. Pseudo–acceleration spectra for γ = 0.30 and different values of α, corresponding to soft soil (zone D).

D), pseudo-acceleration values corresponding to dual systems are lower than the elastic ones, which decrease as the value of α decreases, in general for periods greater than 0.3 s. Pseudo-acceleration values decrease up to 85% with respect to values associated to an elastic behavior due to the energy dissipation in the secondary system, which allows the design of structural systems with hysteretic dampers with forces no greater than the elastic forces. However, it must be verified that both the ductility demand on the structure-dissipater system and on the dissipater itself are within their corresponding allowable limits.

5.4. Influence of Parameters α and γ in the Ratios of UAER Displacement Spectra

Seismic design of structures is commonly performed using design spectra modified by different factors (e.g. over-strength, ductility, etc.). When a structure equipped with hysteretic dissipaters is designed based on displacement control, the design spectrum of displacements can be modified through a damping factor (herein called F_{md}), which considers the energy dissipation given by the dampers (secondary system).

Values of the F_{md} factor are obtained here through ratios of UAER displacement spectra associated to a mean annual exceedance rate $\nu = 0.004$, corresponding to systems with hysteretic dissipaters and UAER spectra of conventional system, assuming a critical damping ratio ξ = 5%, which is expressed as follows:

$$F_{md} = \frac{D_{UAER}(T_1, \alpha, \gamma, \xi = 5\%)}{D_{UAER}(T_1, \xi = 5\%)} \tag{15}$$

where $\mathrm{D_{UAER}}(\mathrm{T}_1, \alpha, \gamma, \xi = 5\%)$ is the UAER spectrum of systems equipped with hysteretic energy dissipaters (dual SDOF system), and $\mathrm{D_{UAER}}(\mathrm{T}_1, \xi = 5\%)$ is the UAER spectrum for conventional systems without energy dissipaters (simple SDOF system).

The calculation of the ratios of UAER displacement spectra (Eq. 15) for different combinations of the dual system given by parameters α and γ (see Table 1) and for the seven zones of CDMX (see Table 3) is done below. Figure 16a–g show the ratios of spectral ordinates of displacement considering α = 0.30 and different values of γ, for the seven zones under study. It is noticed that the *characteristic period* (T_c) is different for each zone, and has a value very close to the dominant period of the soil for the case of soft soils (T_s > 1.0 s). However, for soils with $T_s \leq 1.0$ s, corresponding to zones A (firm ground) and B (medium soil), the *characteristic period* has no relation with the dominant period of the soil. It is noticed also that both the shape and the values of the spectral ratios (Eq. 15) are different for each zone. Therefore, the expressions proposed in the following section have different parameter values, depending on the zone of interest.

6. Mathematical Expressions Proposed for the Spectral Displacement Modification Factor (F_{md})

In order to propose the mathematical expressions for F_{md}, the first necessary step is to obtain all ratios of UAER displacement spectra for different combinations of the dual system, considering parameters α and γ (see Table 1), and for all zones under study (see Table 3). Then, using the spectral ratios, mathematical expressions for the F_{md} factor are fitted through the *least squares method*. The proposed expressions are as follows (Eq. 16):

$$\mathrm{F_{md}} = \begin{cases} a - be^{-\mathrm{c}\left(\frac{\mathrm{T_1}}{\mathrm{T_c}}\right)^{\mathrm{d}}}, & \mathrm{T_s} \leq 0.5s \\ a + \frac{\mathrm{b}\left(\frac{\mathrm{T_1}}{\mathrm{T_c}}\right)^{\mathrm{c}}}{\mathrm{d}+\left(\frac{\mathrm{T_1}}{\mathrm{T_c}}\right)^{\mathrm{c}}}, & \mathrm{T_s} > 0.5s \end{cases} \tag{16}$$

where T_s is the dominant period of the soil in which the structure is located; T_1 is the fundamental vibration period of the structure; values *a*, *b*, and *c* are given by the following expressions:

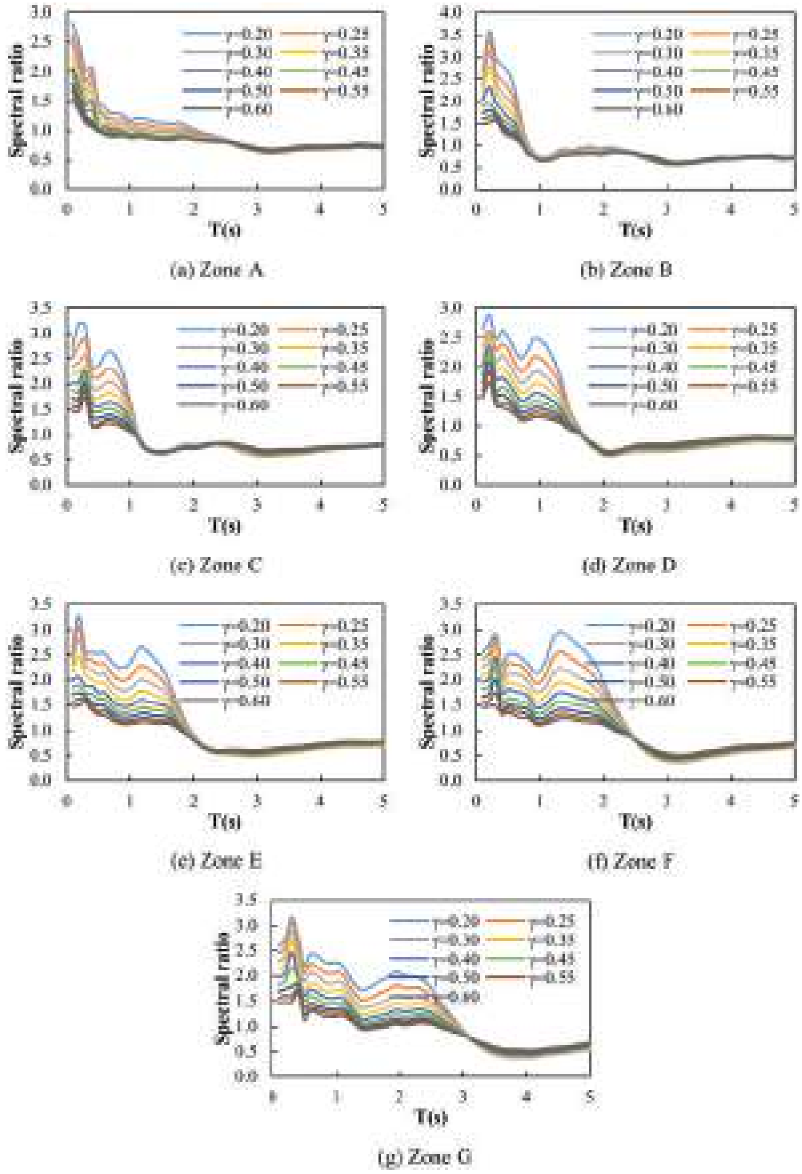

Figure 16. Displacement spectral ratios for α = 0.30 and different values of γ.

$$a = a_1 + a_2\gamma \tag{17}$$

$$b = b_1 + b_2\gamma + \frac{b_3}{\gamma^2} \tag{18}$$

$$c = c_1 + c_2\gamma \tag{19}$$

The values of parameters a_1, a_2, b_1, b_2, b_3, c_1, and c_2 depend on each type of soil, and are a function of parameter α, as shown in Table 4.

The mathematical expressions given by Eq. (16) could be more accurate if more parameters were added with the objective of fitting to the data more closely, but additional parameters would make such

Table 4. Parameter values to estimate F_{md} factor.

Parameter	Soil dominant period (s)						
	$T_s \le 0.5$	$0.5 < T_s \le 1.0$	$1.0 < T_s \le 1.5$	$1.5 < T_s \le 2.0$	$2.0 < T_s \le 2.5$	$2.5 < T_s \le 3.0$	$3.0 < T_s \le 4.0$
T_c	2.6	2.5	1.3	1.8	2.2	2.29 + 0.71α	2.82 + 0.94α
a_1	4.18–0.95α	0.7 + 0.08α	0.56 + 0.3α	0.38 + 0.59α	0.34 + 0.59α	0.25 + 0.57α	0.89α
a_2	1.43–13.62α	−0.22 + 0.67α	0.43α	0.29–0.13α	0.25 + 0.05α	0.12 + 0.67α	0.17 + 0.65α
b_1	3.9–0.82α	4.4–6.5α	4.6–7.8α	4.7–8.5α	4.31–6.9α	4.2–6.5α	6.4–10.6α
b_2	1.85–17.26α	−4.16 + 4.94α	−5.01 + 7.75α	−6.71 + 13.21α	−5.41 + 8.42α	−4.65 + 6.39α	−7.57 + 12.43α
b_3	0	0.04–0.07α	0.03–0.04α	0.03–0.05α	0.03-0.04α	0.06–0.1α	−0.03 + 0.06α
c_1	0.16 + 0.18α	−5.7	−7.07	−8.13	−8.97	−9.77	−4.58
c_2	0.04–0.93α	0	0	0	0	0	0
d	−0.92 + 0.59α	2161	6.35	6.8	5.32	3.49	2.22

expressions more complex. However, the expressions proposed lead to good approximate results, and are useful for the seismic design of structures. As an example, Fig. 17 shows the proposed expressions considering $\alpha = 0.30$ and different values of γ, for the seven zones considered.

7. Illustrative Examples

7.1. Problem Statement

In this section, dual SDOF systems with mass m = 30000 kg, critical damping ratio ξ = 5% in the primary system, stiffness ratio $\alpha = 0.30$, and strength ratio $\gamma = 0.25$, are considered; here, α is the ratio between the stiffness of the primary system k_p and that of the dual system k_t (Eq. 4), and γ is the ratio between the yielding force of dissipater (secondary system) V_{ys} and the yielding force of the dual system V_{yt} (Eq. 5).

It is assumed that the systems are located in three different zones (A, D, F), and for each zone were considered three dual SDOF systems, having three different vibration periods. The systems are subjected to seismic ground motions originated by the events shown in Table 5. The elastic displacement spectra of the seismic motions are shown in Fig. 18. The objective is to obtain the characteristics (stiffness and strength) that both the primary and the secondary system should have in order to get a displacement average no greater than a target maximum value (d_{Target}) (assumed limit displacement corresponding to the yielding displacement of the primary system). For Zone A, it was considered a value of 0.10 cm, of 1.0 cm, and of 2.0 cm, as the maximum target displacement for each system under study. Similarly, for Zone D, values of 0.15 cm, 6.0 cm, and 10.0 cm; and for Zone F, values of 0.20 cm, 10.0 cm, and 15.0 cm. Note that, even that we are dealing with the same seismic events, the maximum target displacement is different in each zone because the displacement demands are also different. To solve the problem, the expressions proposed in the present study are used.

7.2. Solution to the Problem

The first step is to modify, for each zone, the average spectrum of elastic displacements, using F_{md} given by Eq. (16) (see Fig. 19) in order to estimate the inelastic displacements of a dual system associated to $\alpha = 0.30$ and $\gamma = 0.25$. Based on the modified displacement spectrum, it is selected the vibration period that the dual system must have. For instance, for the system located in Zone D, associated with a maximum target displacement of 6.0 cm, the vibration period that the dual system must have is $T_1 = 1.2$ s (see Fig. 19b). Then, both the vibration frequency and the stiffness of the dual system are calculated. $\omega = 2\pi/T_1 = 5.236$ rad/s, and $k_t = \omega^2 m = 8.225$ kN/cm. Using Eqs. (4), (6) and (8), and considering that $V_{yp} = k_p d_{Target}$, both stiffness k and strength V of both primary and secondary system are obtained: $k_p = 2.467$ kN/cm, $k_s = 5.757$ kN/cm, $V_{yp} = 14.804$ kN and $V_{ys} = 4.935$ kN, respectively. Subscripts p and s refer to the primary and secondary systems, respectively. Table 6 shows the characteristics (stiffness and strength) that both the primary and the secondary

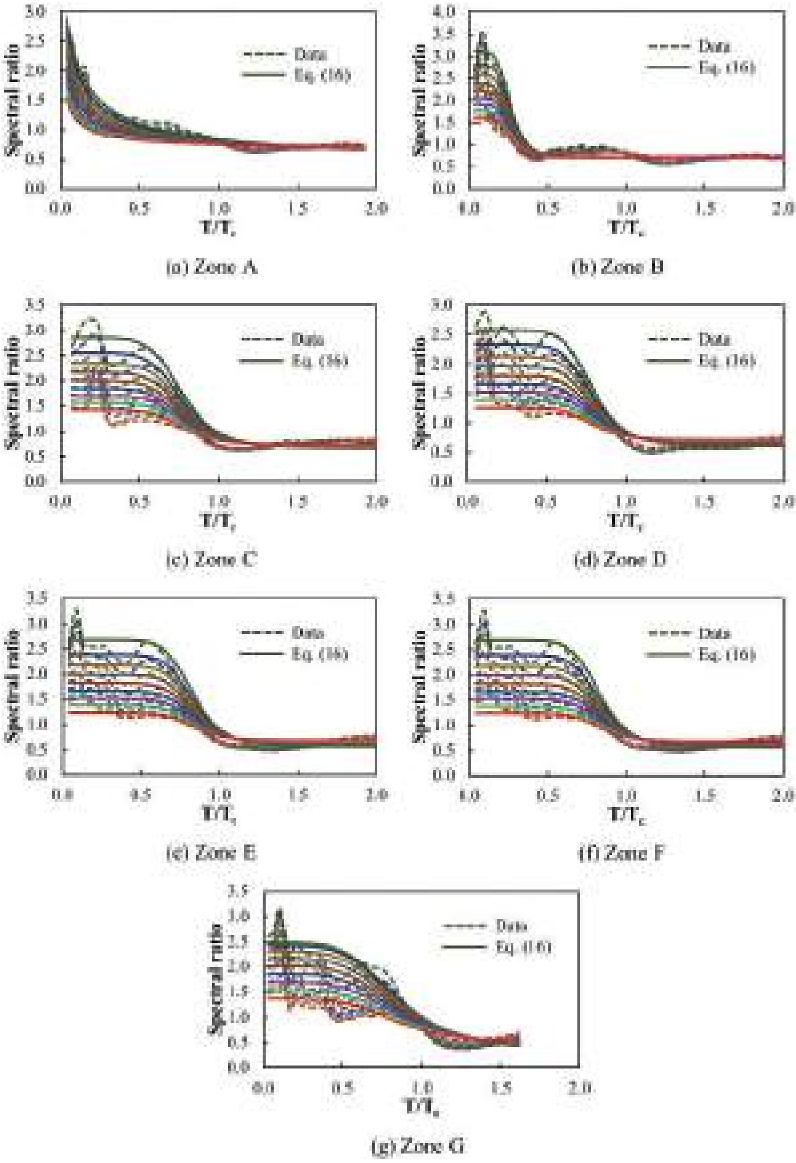

Figure 17. Comparison between spectral ratios, for α = 0.30 and different values of γ.

Table 5. Characteristics of seismic ground motions.

			Coordinates		Station		
Motion	Date	Magnitude	Lat. N	Long. W	Zona A	Zona D	Zona F
S1	18/04/2014	7.3	17.550	101.250	CE18	CJ03	AP68
S2	20/03/2012	7.5	16.600	98.390	CP28	CJ04	BO39
S3	18/04/2014	7.3	17.550	101.250	CP28	CJ04	BO39
S4	08/05/2014	6.5	17.360	100.740	CP28	CJ04	BO39
S5	20/03/2012	7.5	16.600	98.390	CUP5	SCT2	CA59
S6	18/04/2014	7.3	17.550	101.250	CUP5	SCT2	CA59
S7	14/09/1995	7.3	16.730	98.540	CUP5	SP51	CDAO
S8	08/05/2014	6.5	17.360	100.740	FJ74	SP51	JA43

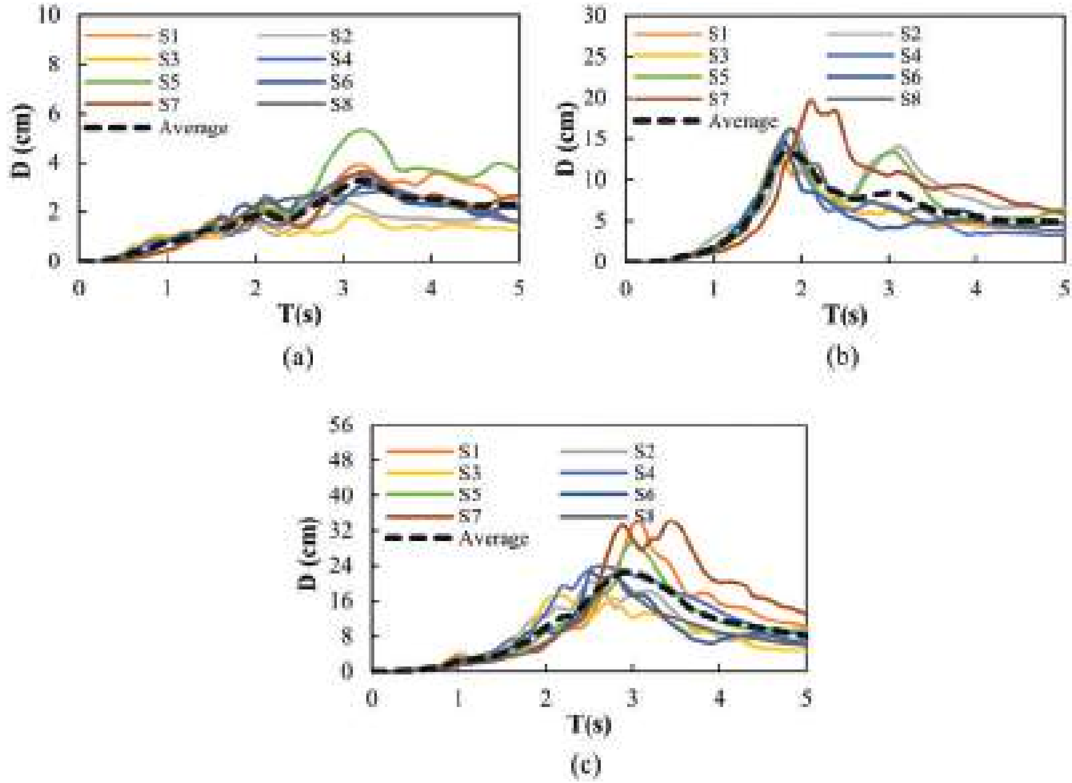

Figure 18. Elastic displacement spectra (ξ = 5%): (a) zone A, (b) zone D, and (c) zone F.

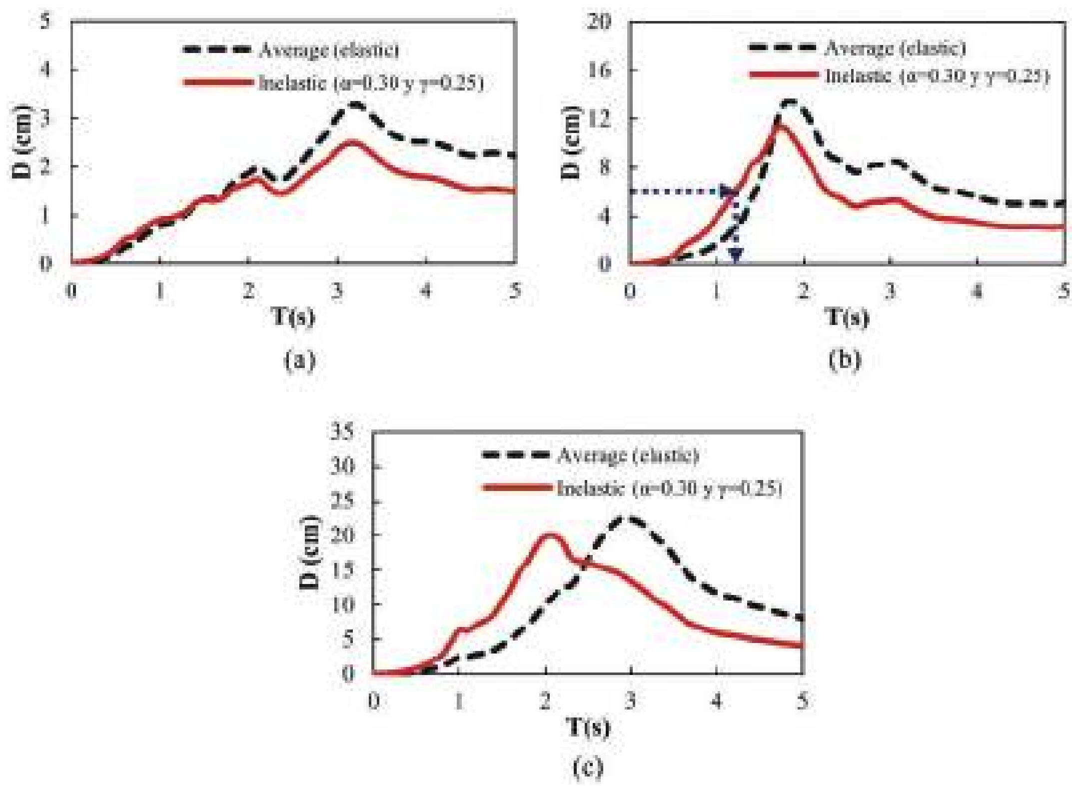

Figure 19. Average spectrum of elastic displacement, and average spectrum modified with expression 16: (a) zone A, (b) zone D, and (c) zone F.

Table 6. Characteristics and displacements of dual SDOF systems.

Zone	System	d_{Target} (cm)	T_1 (s)	k_t (kN/cm)	k_p (kN/cm)	k_s (kN/cm)	V_{yp} (kN)	V_{ys} (kN)	d_{THA} (cm)	Error (%)
A	I	0.1	0.27	162.463	48.739	113.724	4.874	1.625	0.08	20
	II	1.0	1.21	8.089	2.427	5.663	2.427	0.809	0.94	6
	III	2.0	2.79	1.522	0.456	1.065	0.913	0.304	1.74	13
D	I	0.15	0.26	175.200	52.560	122.640	7.884	2.628	0.19	27
	II	6.0	1.20	8.225	2.467	5.757	14.804	4.935	5.26	12
	III	10.0	1.60	4.626	1.388	3.238	13.879	4.626	7.48	25
F	I	0.2	0.27	162.463	48.739	113.724	9.748	3.249	0.19	5
	II	10.0	1.48	5.407	1.622	3.785	16.221	5.407	8.91	11
	III	15.0	1.71	4.050	1.215	2.835	18.226	6.075	10.3	31

system should have in order to get a displacement average no greater than a target maximum value, for the three systems located in the three different zones.

7.3. Verification of the Solutions, Using Time-history Analyses

With the aim of verifying the compliance of the design target displacement of the previous solutions, non-linear time-history analyses (NLTHA), were performed using the seismic motions in Table 5.

Table 6 shows the average peak displacement demands (d_{THA}) estimated from the NLTHA. Also, it shows the errors obtained by the comparison of such results regarding the considered design target displacements (d_{Target}). The minimum and the maximum error was 5% and 31%, respectively. For most cases, it is deduced that the primary system does not reach the inelastic range, because the displacement demand was lower than the target displacement.

It is then concluded that, for these examples, the results obtained using the expressions proposed in the present study (Eq. 16) are acceptable.

8. Conclusions

A methodology based on a probabilistic seismic risk analysis was proposed to obtain mathematical expressions of damping factors (F_{md}) useful to modify the spectral ordinates of elastic displacement due to the presence of hysteretic energy dissipaters in the structural system. Such methodology can be applied to any place in the world. The main results of this study are:

(1) Both structural design parameters and type of soil where the structure is located, have a significant influence in: a) fragility curves, b) mean annual displacement exceedance curves, and c) displacement spectra with uniform annual exceedance rates, of structural systems with hysteretic dissipaters.

(2) It is important for the selection of the design parameters of structure-dissipaters systems to consider the type of soil where they are located. Such selection has the aim of controlling conveniently the displacement levels required in the structural system because when increasing the stiffness ratio (α) and the strength ratio (γ) for a structure located on a certain type of soil, the displacements of the structural system can be decreased. However, the same increase in α and γ for a structure on a different type of soil may result in an increase in the displacement of the structural system. Additionally, it is worth mentioning that soil-structure interaction effects were not considered. Consequently, the results might be different from these here reported.

(3) Mathematical expressions for the damping factors (F_{md}), which depend on the vibration period of the structure, the characteristics of the dual system (structure-dissipater), and the type of soil (firm, transition, soft, etc.) in which the structure is located, were proposed. The factors are useful for displacement-based seismic design of structures with hysteretic energy dissipating devices.

(4) Using illustrative examples, it was shown that, the structural displacement computed with the factor F_{md} proposed in the present study, was close to the average displacement calculated employing time-history analyses.

Acknowledgments

This study was done within projects PAPIIT IN100320 of DGAPA-UNAM. The help of CIRES and II-UNAM in supplying the seismic records used in this study is greatly appreciated. The first and third authors thank CONACyT for the support received during their graduate studies.

Funding

This work was supported by the Dirección General de Asuntos del Personal Académico, Universidad Nacional Autónoma de México (PAPIIT IN100320).

ORCID

Sonia E. Ruiz http://orcid.org/0000-0002-2731-6780
Ali Rodríguez-Castellanos http://orcid.org/0000-0002-2068-8194

References

Abdollahzadeh, B., Elkaee, and A. Esmaeelnia. 2012. Response modification factor of dual moment-resistant frame with buckling restrained brace (BRB). *Proc. of the 15th World Conference on Earthquake Engineering*. Lisboa.

American Society of Civil Engineers. 2016. Minimum design loads for buildings and other structures. *ASCE Standard, ASCE 7-16*. Reston, Virginia, United States.

Arroyo-Espinoza, D., and A. Terán-Gilmore. 2002. Factores de reducción de fuerzas sísmicas para el diseño de estructuras con sistemas pasivos de disipación de energía. *Revista de Ingeniería Sísmica* 66: 73–93. doi: 10.18867/ris.66.197.

Asgarian, B., and H. R. Shokrgozar. 2009. BRBF response modification factor. *Journal of Constructional Steel Research* 65: 290–98. doi: 10.1016/j.jcsr.2008.08.002.

Ashour, S. A. (1987) "Elastic seismic response of buidings with supplemental damping," Ph.D. thesis, Civil Engineering Dept., Michigan University.

Baber, T. T., and Y. K. Wen. 1981. Random vibration of hysteretic, degrading systems. *Journal of the Engineering Mechanics Division* 107: 1069–87. doi: 10.1061/JMCEA3.0002768.

Baker, J. W., and C. A. Cornell. 2005. A vector-valued ground motion intensity measure consisting of spectral acceleration and epsilon. *Earthquake Engineering and Structural Dynamics* 34: 1193–217. doi: 10.1002/eqe.474.

Bojorquez, E., R. Chávez, A. Reyes-Salazar, S. E. Ruiz, and J. Bojorquez. 2017. A new motion intensity measure IB. *Soil Dynamics and Earthquake Engineering* 99: 97–107. doi: 10.1016/j.soildyn.2017.05.011.

Bommer, J. J., A. S. Elnashai, and A. G. Weir. 2000. Compatible acceleration and displacement spectra for seismic design codes. *Proc. of the 12th World Conference on Earthquake Engineering*. Auckland.

Bommer, J. J., and R. Mendis. 2004. Scaling of spectral displacement ordinates with damping ratios. *Earthquake Engineering & Structural Dynamics* 34: 145–65. doi: 10.1002/eqe.414.

Building Center of Japan. 1997. *Structural provisions for building structures*. Tokyo: BCJ.

Cameron, J. B., N. Makris, and I. D. Aiken. 2004. Component testing, seismic evaluation and characterization of buckling-restrained braces. *Journal of Earthquake Engineering* 130 (6): 880–94.

Cameron, W. I., and R. A. Green. 2007. Damping correction factors for horizontal ground-motion response spectra. *Bulletin of the Seismological Society of America* 97 (3): 934–60. doi: 10.1785/0120060034.

Casciati, F., and L. Faravelli. 1991. *Fragility analysis of complex structural systems*. Taunton, UK: Research Studies Press.

Castaldo, P., B. Palazzo, and T. Ferrentino. 2016. Seismic reliability-based ductility demand evaluation for inelastic base-isolated structures with friction pendulum devices. *Earthquake Engineering and Structural Dynamics* 46 (8): 1245–66. doi: 10.1002/eqe.2854.

Castaldo, P., E. Tubaldi, F. Selvi, and L. Gioiella. 2021. Seismic performance of an existing RC structure retrofitted with buckling restrained braces. *Journal of Building Engineering* 33: 101688. doi: 10.1016/j.jobe.2020.101688.

Castaldo, P., and G. Alfano. 2020. Seismic reliability-based design of hardening and softening structures isolated by double concave sliding devices. *Soil Dynamics and Earthquake Engineering* 129: 105930. doi: 10.1016/j.soildyn.2019.105930.

Castillo, T., and S. E. Ruiz. 2013. Factor de reducción por amortiguamiento para el diseño sísmico de estructuras con disipadores de energía. In *Serie Azul*, 682. Instituto de Ingeniería, Universidad Nacional Autonoma de Mexico, Ciudad Universitaria, Ciudad de México, México.

Castillo, T., and S. E. Ruiz. 2014. Reduction factors for seismic design spectra for structures with viscous energy dampers. *Journal of Earthquake Engineering* 18 (3): 323–49. doi: 10.1080/13632469.2013.860932.

Comité Européen de Normalisation (CEN). 2004. *Eurocode 8: Design of structures for earthquake resistance-Part 1: General rules, seismic actions and rules for buildings*. Brussels, Belgium: CEN 2004-1-1, CEN.

Cornell, C. A. 1968. Engineering seismic hazard analysis. *Bulletin of the Seismological Society of America* 58 (5): 1583–606.

Domínguez, D., and F. López-Almansa (2017) "Feseability of hysteretic energy dissipators for bulk seismic protection of vulnerable buildings in chile," *Proc. of the 16th World Conference on Earthquake Engineering*, Santiago de Chile, Chile.

Esteva, L. 1967. Criterio para la construcción de espectros de espectros para diseño sísmico. *Proceedings of XII Jornadas Sudamericanas de Ingeniería Estructural y III Simposio Panamericano de Estructuras*, Caracas, Venezuela. Published later in Boletín del Instituto de Materiales y Modelos Estructurales, Universidad Central de Venezuela, No. 19, 1967.

FEMA. 2018. *Seismic performance assessment of buildings. Volume 1-Methodology*. Washington, D.C: FEMA P-58-1, prepared by the Applied Technology Council for the Federal Emergency Management Agency.

Fukuyama, H., and S. Sugano. 2000. Japanese seismic rehabilitation of concrete buildings after the Hyogoken-Nanbu Earthquake. *Cement and Concrete Composites* 22: 59–79. doi: 10.1016/S0958-9465(99)00042-6.

Greco, R., A. Fiore, and B. Briseghella. 2018. Influence of soil type on damping reduction factor: A stochastic analysis based on peak theory. *Soil Dynamics and Earthquake Engineering* 104: 365–68. doi: 10.1016/j.soildyn.2017.10.020.

Guerrero, H., T. Ji, A. Terán-Gilmore, and J. A. Escobar. 2016. A method for preliminary seismic design and assessment of low-rise structures protected with buckling restrained braces. *Engineering Structures* 123: 141–54. doi: 10.1016/j.engstruct.2016.05.015.

Hatzigeorgiou, G. D. 2010. Damping modification factors for SDOF systems subjected to near-fault, far-fault and artificial earthquakes. *Earthquake Engineering and Structural Dynamics* 39 (11): 1239–58. doi: 10.1002/eqe.991.

Hazaveh, N., G. W. Rodgers, S. Pampanin, and J. G. Chase. 2016. Damping reduction factors and code-based design equation for structures using semi-active viscous dampers. *Earthquake Engineering and Structural Dynamics* 45 (15): 2533–50. doi: 10.1002/eqe.2782.

Hidalgo, J. P., and S. E. Ruiz. 2010. Factor de reducción β por incremento de amortiguamiento viscoso, para estructuras desplantadas sobre roca. *Revista de la Sociedad Mexicana de Ingeniería Sísmica* 83: 1–23.

Hurtado, F., and L. M. Bozzo (2008) "Numerical and experimental analysis of a shear-link energy dissipator for seismic protection of buildings," *Proc. of the 14th World Conference on Earthquake Engineering*, Beijing, China.

Inoue, K., and S. Kuwara. 1998. Optimum strength ratio of hysteretic damper. *Earthquake Engineering Structural Dynamics* 27 (6): 578–88. doi: 10.1002/(SICI)1096-9845(199806)27:6<577::AID-EQE743>3.0.CO;2-U.

Kawashima, K., and K. Aizawa 1986 Modification of earthquake response spectra with respect to damping ratio. *Proc. of the 3rd US National Conference on Earthquake Engineering*,Vol. 2. Charleston, South Caroline.

Kim, J., and Y. Seo. 2004. Seismic design of low-rise steel frames with buckling-restrained braces. *Engineering Structures* 26: 543–51. doi: 10.1016/j.engstruct.2003.11.005.

Liu, B., M. Liu, and Y. Li (2004) "Research and development of performance-based seismic design theory," *Proc. of the 13th World Conference on Earthquake Engineering* (CD-ROM), Canadian Association for Earthquake Engineering, Vancouver, Canada.

Maley, T., T. Sullivan, and G. Della Corte. 2010. Development of a displacement-based design method for steel dual systems with buckling-restrained braces and moment-resisting frames. *Journal of Earthquake Engineering* 14 (S1): 106–40. doi: 10.1080/13632461003651687.

Merritt, S., C. Uang, and G. Benzoni. 2003. Subassemblage testing of corebrace buckling-restrained braces. *Report No. TR-2003/01*. San Diego, USA: Department of Structural Engineering, University of California.

Mexico City Building Code (MCBC). 2017. Reglamento de Construcciones para el Distrito Federal. *Gobierno de la Ciudad de México*, México: MCBC 2017.

Moehle, J., and G. G. Deierlein. 2004. A framework methodology for performance-based earthquake engineering. *Proc. of the 13th World Conference on Earthquake Engineering* (CD-ROM). Vancouver, Canada: Canadian Association for Earthquake Engineering.

Mollaioli, F., L. Liberatore, and A. Lucchini. 2014. Displacement damping modification factors for pulse-like and ordinary records. *Engineering Structures* 78: 17–27. doi: 10.1016/j.engstruct.2014.07.046.

Naeim, F., and C. A. Kircher. 2001. On the damping adjustment factors for earthquake response spectra. *The Structural Design of Tall Buildings* 10: 361–69. doi: 10.1002/tal.180.

Nagao, K., and J. Kanda. 2015. Estimation of damping correction factors using duration defined by the standard deviation of phase difference. *Earthquake Spectra* 31 (2): 761–83. doi: 10.1193/103012EQS321M.

Nakashima, M., K. Saburi, and B. Tsuji. 1996. Energy input and dissipation behavior of structures with hysteretic dampers. *Earthquake Engineering & Structural Dynamics* 25 (5): 483–96. doi: 10.1002/(SICI)1096-9845(199605)25:5<483::AID-EQE564>3.0.CO;2-K.

National Research Council of Canada. 2010. *National Building Code of Canada*. Ottawa, Canada: NRCC 2010.
Ordaz, M., and C. Montoya. 2014. DEGTRA 9.3.2. In *Software*, México: Instituto de Ingeniería, Universidad Nacional Autónoma de México.
Palazzo, B., P. Castaldo, and I. Marino. 2015. The dissipative column: A new hysteretic damper. *Buildings* 5 (1): 163–78. doi: 10.3390/buildings5010163.
Palermo, M., S. Silvestri, and T. Trombetti. 2016. Stochastic-based damping reduction factors. *Soil Dynamics and Earthquake Engineering* 180: 168–76. doi: 10.1016/j.soildyn.2015.09.014.
Papagiannopoulos, G. A., G. D. Hatzigeorgiou, and D. E. Beskos. 2013. Recovery of spectral absolute acceleration and spectral relative velocity from their pseudo-spectral counterparts. *Earthquakes and Structures* 4 (5): 489–508. doi: 10.12989/eas.2013.4.5.489.
Priestley, M. J. N., G. M. Calvi, and Kowalsky. 2007. *Displacement-based design of structures*. Pavia, Italy: IUSS Press.
Rivera, J. L., and S. E. Ruiz. 2007. Design approach based on UAFR spectra for structures with displacement-dependent dissipating elements. *Earthquake Spectra* 23l (2): 417–39. doi: 10.1193/1.2722380.
Rosenblueth, E., and L. Esteva. 1972. Reliability basis for some Mexican codes. *ACI* SP-31: 1–41.
Ruiz, S. E., and H. Badillo. 2001. Performance-Based design approach for seismic rehabilitation of buildings with displacement-dependent dissipaters. *Earthquake Spectra* 17 (3): 531–48. doi: 10.1193/1.1586187.
Ruiz, S. E., M. A. Santos-Santiago, E. Bojórquez, M. A. Orellana, F. Valenzuela-Beltrán, J. Bojórquez, and M. Barraza. 2021. BRB retrofit of mid-rise soft-first-story RC moment-frame buildings with masonry infill in upper stories. *Journal of Building Engineering* 38: 101783. doi: 10.1016/j.jobe.2020.101783.
Segovia, V., and S. E. Ruiz. 2017. Direct displacement-based design for buildings with hysteretic dampers, using best combinations of stiffness and strength ratios. *Journal of Earthquake Engineering* 21 (5): 752–75. doi: 10.1080/13632469.2016.1185054.
Shome, N., and C. A. Cornell. 1999. Probabilistic Seismic Demand Analysis of Nonlinear Structures. *Report No. RMS-35*. Stanford, USA: Department of Civil and Environmental Engineering, Stanford University
Silva, F. L., and S. E. Ruiz. 2000. Calibration of the equivalent linearization method applied to simple hysteretic systems subjected to narrow band motions. *Structural Safety* 22 (3): 211–31. doi: 10.1016/S0167-4730(00)00007-2.
Singh, S. K., V. Cruz-Atienza, X. Pérez-Campos, A. Iglesias, V. Hjörleifsdóttir, E. Reinoso, M. Ordaz, and D. Arroyo. 2018. Deadly intraslab Mexico earthquake of 19 September 2017 (Mw 7.1): Ground motion and damage pattern in Mexico City. *Seismol. Res. Lett* 89 (6): 2193–203. doi: 10.1785/0220180159.
Sues, R. H., S. T. Mau, and Y. K. Wen. 1988. Systems identification of degrading hysteretic restoring forces. *Journal of Engineering Mechanics* 114 (5): 833–46. doi: 10.1061/(ASCE)0733-9399(1988)114:5(833).
Symans, M. D., F. A. Charney, A. S. Whittaker, M. C. Constantinou, C. A. Kircher, M. W. Johnson, and R. J. McNamara. 2008. Energy dissipations systems for seismic applications: Current practice and recent developments. *Journal of Structural Engineering* 134 (1): 3–21. doi: 10.1061/(ASCE)0733-9445(2008)134:1(3).
Takeuchi, T. 2018. Buckling-Restrained Brace: History, desing and applications. *Key Engineering Materials* 763: 50–60. doi: 10.4028/www.scientific.net/KEM.763.50.
Teran-Gilmore, A., and N. Virto-Cambray. 2009. Preliminary design of low-rise buildings stiffened with buckling-restrained braces by a displacement-based approach. *Earthquake Spectra* 25 (1): 185–211. doi: 10.1193/1.3054638.
Tolis, S. V., and E. Faccioli. 1999. Displacement design spectra. *Journal of Earthquake Engineering* 3: 107–25. doi: 10.1080/13632469909350342.
Vargas, R., and M. Bruneau. 2009. Analytical response and design of buildings with metallic structural fuses I. *Journal of Structural Engineering* 135 (4): 386–93. doi: 10.1061/(ASCE)0733-9445(2009)135:4(386).
Vargas, R. E., and M. Bruneau. 2006. Analytical Investigation of the Structural Fuse Concept. *Technical Report MCEER-06-0004*. New York, USA. Department of Civil, Structural and Environmental Engineering, University at Buffalo.
Yang, T. Y., J. Moehle, B. Stojadinovic, and A. D. Kiureghian. 2009. Seimic performance evaluation of facilities: Methodology and implementation. *Journal of Structural Engineering* 135 (10): 1146–54. doi: 10.1061/(ASCE)0733-9445(2009)135:10(1146).
Zeng, X., X. Lu, T. Y. Yang, and Z. Xu. 2016. Application of the FEMA-P58 methodology for regional earthquake loss prediction. *The Structural Design of Tall and Special Buildings* 21: 578–91.
Zhou, F., L. Wenguang, and Z. Xu. 2003. Satate of the art on applications, R&D and design rules for seismic isolation in China. *Proc. of the 8th World Seminar on Seismic Isolation, Energy Dissipation and Active Vibration Control of Structures*. 113–21. Yerevan, Armenia.
Zhou, J., and J. X. Zhao. 2020. A damping modification factor prediction model for horizontal displacement spectrum from subduction slab earthquakes in Japan accounting for site conditions. *Bulletin of the Seismological Society of America* XX: 1–19.